Annual Report of 2003 Proposal:

Proposal Title:
Seismic study of the San Andreas fault at Parkfield and the Superstition Hills fault in Imperial Valley.

Proposal Category: Data Gathering and Products.

Disciplinary Committee: Seismology; Fault and Rock Mechanics.

Focus Group: Earthquake Source Physics

Principal Investigators: Yong-Gang Li at USC

Scientific Results:

I. Through fault-zone trapped wave data collection at dense linear seismic arrays deployed across and along the San Andreas fault near Parkfield and quantitative analysis and modeling of the data, we characterize the dimensions and magnitude of the highly damaged core zone on the SAF at Parkfield. The zone on the SAF main fault is marked by a low-velocity waveguide ~150 m wide, to a depth of at least 5 km, in which *Q* is 15-50 and *S* velocities are reduced by 30-40% from wall-rock velocities. The waveguide is not uniform at depth and along the fault. We interpret this distinct low-velocity core zone was formed by repeated damage during recurrent *M*6 earthquakes and other large earthquakes on the principal slip plane at Parkfield. A less-developed low-velocity zone (with velocity reduction of 20% and width of 50 m) may exist on the north strand at the array site, which experienced minor surface breaks in the 1966 *M*6 event, most likely due to secondary slip and strong shaking from ruptures on the main fault. The width of the low-velocity waveguide inferred by trapped waves likely represents the macroscopic damage extent in dynamic rupture and microscopic fault process zone accumulating mechanical, chemical, thermal, and other kinematical processes. The variation in velocity reduction within the waveguide along the fault zone and with depth may be caused by changes in overburden pressure, rock type, stress and slip rate, fault geometry, fluid content, and dynamic rupture during past earthquakes. A high-resolution image of internal structure and physical properties of the SAF enable us to better understand the state of active faults and the earthquake behavior on them as well as the relationship between the fault zone structure and dynamic rupture. The preliminary results from this study are included in our recent manuscript "Low-velocity damaged structure of the San Andreas fault at Parkfield from fault-zone trapped waves, SAFOD I: Results from pre-drilling site characterization studies at Parkfield" that has been submitted to Special Section I of SAFOD I, *Geophy. Res. Lett.*, 2003. The manuscript is attached in this report.

II. Observations and modeling of fault-zone trapped waves recorded at rupture zone of the 1987 *M*6.6 Superstition Hills earthquake have allowed us to obtain additional details of the inner damage zone at the fault segments with different slip patterns. Numerical simulations of trapped waves from explosions and microearthquakes show an ~75-m-wide low-velocity waveguides on the Superstition Hills fault (SHF) where shear velocities are reduced by 25-30% from wall-rock velocities and *Q* values of 10-50 between the surface and seismogenic depth. Compared with the southeast rupture segment, the northwest segment inferred by trapped waves is characterized by a relatively simple waveguide narrower and with greater velocity reduction, likely corresponding to the rapid rupture and larger slip on this segment in the 1987 earthquake. The strong motion recordings for the sub-event on the northwest rupture segment showed the higher frequency contents. On the other hand, the waveguide on the southeast rupture segment is more complicated in a broad zone, which might be due to the multiple subsurface fault strands on the southwest side of the main fault trace according to the post-seismic displacement measurements. The results from trapped waves also suggest that the two fault segments connect at seismogenic depth although they are apart about 100-200 m at surface in the stepover feature. This tree-like branching of the fault zone is also shown in the high-resolution reflection profile at the SHF by R. Catchings and M. Rymer of USGS. Combined with results from reflection imaging with fault-zone guided wave delineation of the SHF, a manuscript is in writing and will be submitted soon.

Appendix:

Low-Velocity Damaged Structure of the San Andreas Fault at Parkfield from Fault-Zone Trapped Waves

Yong-Gang Li, John E. Vidale and Elizabeth S. Cochran

Abstract. We used dense linear seismic arrays across and along the San Andreas fault (SAF) at Parkfield, California to record fault-zone trapped waves generated by explosions and microearthquakes in 2002. Prominent trapped waves with large amplitudes and long duration appeared at stations close to the SAF main fault trace while some energy was trapped in the north strand at the array site. Observations and 3-D finite-difference simulations of trapped waves at 2-5 Hz show evidence of a damaged core zone on the main SAF. The zone from the surface to seismogenic depths is marked by a low-velocity waveguide ~150 m wide, in which *Q* is 10-50 and shear velocities are reduced by 30-40% from wall-rock velocities, with the greatest velocity reduction at shallow depth. We interpret that this distinct low-velocity zone on the main SAF is a remanent of repeated damage due to *M*6 episode and historical large earthquakes on the principal fault plane at Parkfield. A less-developed low-velocity zone may be evident on the north strand that experienced minor breaks in the 1966 *M*6 event.

Introduction

Mature faults are planes of weakness in the Earth crust. They facilitate slip under the prevailing stress orientation. Field evidence shows that the rupture plane of slip on a mature fault tends to exist on the edge of damage zone at the plane of contact with the intact wall rock. High-resolution delineation of the internal structure of the SAF and monitoring microseismic events that occur close to or on the principal slip plane thus may be crucial for earthquake predication. The combination of multiple planes on the primary fault and other fault-related structures make imaging an internal structure like the SAF challenging.

At Parkfield, seismological studies have revealed a low-velocity zone surrounding the surface trace of the SAF [e.g. *Lees and Malin*, 1990; *Michelini and McEvilly*, 1991; *Thurber et al.*, 1997; *Hole et al.*, 2001]. This zone is a few hundreds of meters to km wide with velocity reductions of 10-30% and *Vp/Vs* ratios of 2.3. The low *Vs* and corresponding high *Vp/Vs* ratios within the fault zone are interpreted to be caused by dilatant fracturing due to high pore-fluid pressures. Magnetotelluric imaging of the SAF at Parkfield yields a similar model, with a zone of very low resistivity a few hundred meters wide extending to a depth at least 3-4 km [*Unsworth et al.*, 1997]; the low-resistivity zone is interpreted to be fluid-rich. *Byerlee* [1990], and *Rice* [1992] note that the high pore-pressures within a fault
zone at seismogenic depths may be due in part to its greater permeability than adjacent blocks. Our previous studies at the Parkfield SAF using fault-zone trapped waves generated by earthquakes and explosions suggests that the fault zone includes a 100- to 160-m-wide damaged core layer, in which velocities are reduced by 30-40% and *Q* is ~30 [*Li et al.*, 1990; *Li et al.*, 1997]. New data recorded in an extensive experiment conducted at the SAF, Parkfield in Fall 2002 allow us to characterize the internal structure and damage extent of the fault zone with higher-resolution.

Data and Results

We deployed 54 three-component seismometers on 3 dense seismic lines along and across surface traces of the SAF, ~15 km southeast of the drilling site of San Andreas Fault Observatory at Depth (SAFOD), and detonated 3 explosions, each using 250 kg of chemical explosives in a 33-m-deep hole, within and outside the fault zone at Parkfield (Figure 1). Array A was 850-m-long across the SAF. Arrays B and C were 400-m along the main and north fault strands, respectively. The seismic arrays operated for a month to record earthquakes and explosions, including our 3 shots and a dozen smaller shots detonated around the SAFOD drilling site in the PASO experiment [*Thurber and Roecker*, 2002]. Figure 2a shows seismograms recorded at array A for the 3 explosions and an *M*1.5 earthquake. For shots PARK and PMM, and the quake located on the SAF (Figure 1), we observe fault-zone trapped waves with large amplitudes and long-duration wavetrains following *S* waves at stations between E4 and W4 close to the main fault trace. The amplitude of trapped waves decrease away from the fault. However, for shot PRIS located 4 km away from the fault (Figure 1), trapped waves are not obvious on any station, and *P* waves dominate in the profile. These observations

show the existence of a low-velocity waveguide along the main fault, which is approximately 150 to 200 m wide where trapped waves are dominant. We note that trapped waves from shot PARK located 4.2 km SE of the array traveled slower and more concentrated in the fault zone than those from shot PMM 7 km NW of the array, indicating heterogeneity in velocity and width of the waveguide. Seismic waves from the *M*1.5 earthquake at 5 km depth and 20 km NW of the array traveled faster than those from the near-surface shots, further suggesting that the fault zone has lower velocities at shallower depths. Some trapped energy with a short wavetrain following *S* is noticeable at stations on the north fault strand for this quake. We infer a weak waveguide less velocity reduction on the north strand that connects to the main fault at depth NW of the array, and acts to partition some guided energy.

Figure 2b shows seismograms recorded on array B along the main fault for shots PARK and LCCB detonated within and 3 km away from the SAF, respectively. Trapped waves generated by shot PARK show coherent phase with large amplitudes after *S* waves. In contrast, *P* waves dominant in the profile for shot LCCB. In order to eliminate site effects on fault-zone trapped waves, we compute amplitude ratios of trapped waves to *P* waves at all stations for 14 events located within and away from the SAF (Figure 1). The amplitudes are computed in 2 s time windows that include *P* and dominant trapped waves, respectively, in low-pass (<5 Hz) filtered seismograms. Figure 3 shows the maximum amplitude ratio at the SAF main fault, which decreases rapidly away from the main fault, although a second peak is seen at the north strand for in-fault events. In contrast, amplitude ratios for events far from the SAF are low and flat across the fault zone because they did not trap significant energy.

We have modeled the fault-zone trapped waves using a 3-D finite-difference code [*Graves*, 1996], resulting in a velocity and *Q* section across the fault to a depth of 5 km, for the structure of the SAF near Parkfield. We first synthesize fault-zone trapped waves generated by the near-surface explosions to determine the shallowest 1 or 2 km fault zone structure. We interpret that the later wavetrain of trapped waves in explosion profiles traveled in the top layer while the early wavetrain penetrated lower layers. Synthetic seismograms were fit to the later trapped wavetrain first and then the early trapped wavetrain was fit in forward modeling. Thus we stripped shallow effects to resolve deeper structure of the fault zone. We then synthesized trapped waves from the earthquake at seismogenic depths to complete a model of the SAF with depth-variable structure in 3-D, including low-velocity waveguides on the main and north fault strands (Figure 4a, b). In grid-search modeling, we tested various values for fault zone width, velocity, *Q* value, layer depth, and source location. We also use velocities from seismic profiling of the shallow SAF at Parkfield [*Catchings et al*., 2002] as constraints. The best-fit model parameters are shown in Table 1.

Table 1 Model Parameters for the SAF near Parkfield

Parameters Layer No.	1	2	3	4
Main fault NW/SE of array A:				
Depth of the layer, km	0.25	1.0	2.0	5.0
Waveguide width, m	175/150	175/150	150/125	125/100
Waveguide *Vs*, km/s	0.5/0.35	0.65/0.55	1.0/0.9	1.7/1.4
Waveguide *Vp*, km/s	1.3	1.8	2.3/2.1	3.5/3.0
Waveguide *Q*	10	25	30	50
NE wall-rock *Vs*, km/s	0.8/0.6	1.0/0.9	1.5/1.4	2.3/2.0
NE wall-rock *Vp*, km/s	2.0/1.5	2.5/2.2	3.3/3.0	5.0/4.2
SW wall-rock *Vs*, km/s	0.8/0.6	1.0/0.9	1.6/1.5	2.5/2.2
SW wall-rock *Vp*, km/s	2.0/1.5	2.5/2.2	3.5/3.2	5.2/4.5
Wall rock *Q* 20	50	60	100	
North fault strand:				
Waveguide width, m	50	50	50	50
Waveguide *Vs*, km/s	0.65	0.8	1.3	2.0
Waveguide *VP*, km/s	1.6	2.0	2.8	4.0
Waveguide *Q*	30	40	50	

A good agreement of synthetic trapped waveforms with observations are obtained for explosions and earthquakes using the depth-dependent fault-zone structural model shown in Figure 4a and Table 1. Figure 4c exhibits observed and synthetic seismograms at array B for shot PMM. Fault-zone trapped waves with large amplitudes, long duration, and slightly dispersive wavetrains follow *S* waves. Figure 4d shows observed and synthetic seismograms at 9 stations of array A close to the SAF main fault for shots PMM and PARK. Fault-zone trapped waves are dominant at these stations. Figure 4e exhibits observed and synthetic seismograms at array A for the *M*1.5 quake occurring at the 5 km

depth. Trapped waves are seen at stations close to the main fault on which a well-developed low-velocity waveguide exists. Some trapped energy with smaller amplitudes and shorter wavetrains appeared at the north strand, on which a less-developed waveguide probably exists. The numerical simulations give a good fit to observations although the recorded seismograms show more scattered waves. We tested various fault zone depths in modeling. For example, synthetic seismograms generated by the *M*1.5 event for a 1-km-deep low-velocity fault zone could not match observed guided waves with long-duration wavetrains although the *S* waves did have greater amplitudes within the shallow fault zone than outside the fault zone.

Discussions and Conclusions

Through fault-zone trapped wave data collection and analysis, we quantitatively characterize the dimensions and magnitude of the highly damaged core zone on the SAF at Parkfield. The zone on the main fault is marked by a low-velocity waveguide ~150 m wide, to a depth of at least 5 km, in which *Q* is 15-50 and *S* velocities are reduced by 30-40% from wall-rock velocities. The waveguide is not uniform at depth and along the fault. Additional deeper events would help to document the deep part of the fault zone. We interpret this distinct low-velocity core zone was formed by repeated damage during recurrent *M*6 earthquakes and other large earthquakes on the principal slip plane at Parkfield. A less-developed low-velocity zone (with velocity reduction of 20% and width of 50 m) may exist on the north strand at the array site, which experienced minor surface breaks in the 1966 *M*6 event, most likely due to secondary slip and strong shaking from ruptures on the main fault. The width of the low-velocity waveguide inferred by trapped waves likely represents the macroscopic damage extent in dynamic rupture and microscopic fault process zone accumulating mechanical, chemical, thermal, and other kinematical processes. The variation in velocity reduction within the waveguide along the fault zone and with depth may be caused by changes in overburden pressure, rock type, stress and slip rate, fault geometry, fluid content, and dynamic rupture during past earthquakes. A high-resolution image of the SAF enable us to better understand the relationship between the fault zone structure and dynamic rupture.

References

Beck, S. L. and D. H. Christensen, Rupture process of the February 4, 1965, Rat Islands earthquake, *J. Geophys. Res.*, *96*, 2205-2221, 1991.

Byerlee, J., Friction, overpressure and fault-normal compression, *Geophys. Res. Lett.*, *17*, 2109-2112, 1990.

Catchings, R. D., M. J. Rymer, M. R. Goldman, J. A. Hole, R. Huggings, and C. Lippus, High-resolution seismic velocities and shallow structure of the San Andreas fault zone at Middle Mountain, Parkfield, California, *Bull. Seismol. Soc. Am.*, 92, 2493-2503, 2002.

Graves, R. W., Simulating seismic wave propagation in 3D elastic media using staggered-grid finite differences, *Bull. Seismol. Soc. Am.*, *86*, 1091-1106, 1996.

Hole, J. A., R. D. Catchings, K. C. St. Clair, M. J. Rymer, D. A. Okaya, and B. J. Carney, Steep-dip seismic imaging of the shallow San Andreas fault near Parkfield, *Science*, 294, 1513-1515, 2001.

Lees, J. M., and P. E. Malin, Tomographic images of *P* wave velocity variation at Parkfield, California, *J. Geophys. Res.*, *95*, 21,793-21,804, 1990.

Li, Y. G., P. C. Leary, K. Aki, and P. E. Malin, Seismic trapped modes in Oroville and San Andreas fault zones, *Science*, *249*, 763-766, 1990.

Li, Y. G., W. L. Ellsworth, C. H. Thurber, P. E. Malin, and K. Aki, Observations of fault-zone trapped waves excited by explosions at the San Andreas fault, central California, *Bull. Seism. Soc. Am.*, 87, 210-221, 1997.

Michelini, A., and T. V. McEvilly, Seismological studies at Parkfield, I, Simultaneous inversion for velocity structure and hypocenters using cubic B-splines parameterization, *Bull. Seismol. Soc. Am.*, *81*, 524-552, 1991.

Rice, J. R., Fault stress states, pore pressure distributions, and the weakness of the San Andreas fault, in *Fault Mechanics and Transport Properties of Rocks*, edited by B. Evans and T.-F. Wong, pp. 475-503, Academic, San Diego, Calif., 1992.

Thurber, C. H., S. Roecker, W. Ellsworth, Y. Chen, W. Lutter, and R. Sessions, Two-dimensional seismic image of the San Andreas fault in the northern Gabilan Range, central California: Evidence for fluids in the fault zone, *Geophys. Res. Lett.*, *24*, 1591-1594, 1997.

Unsworth, M., P. Malin, G. Egbert, and J. Booker, Internal structure of the San Andreas fault at Parkfield, CA, *Geology*, 356-362, 1997.

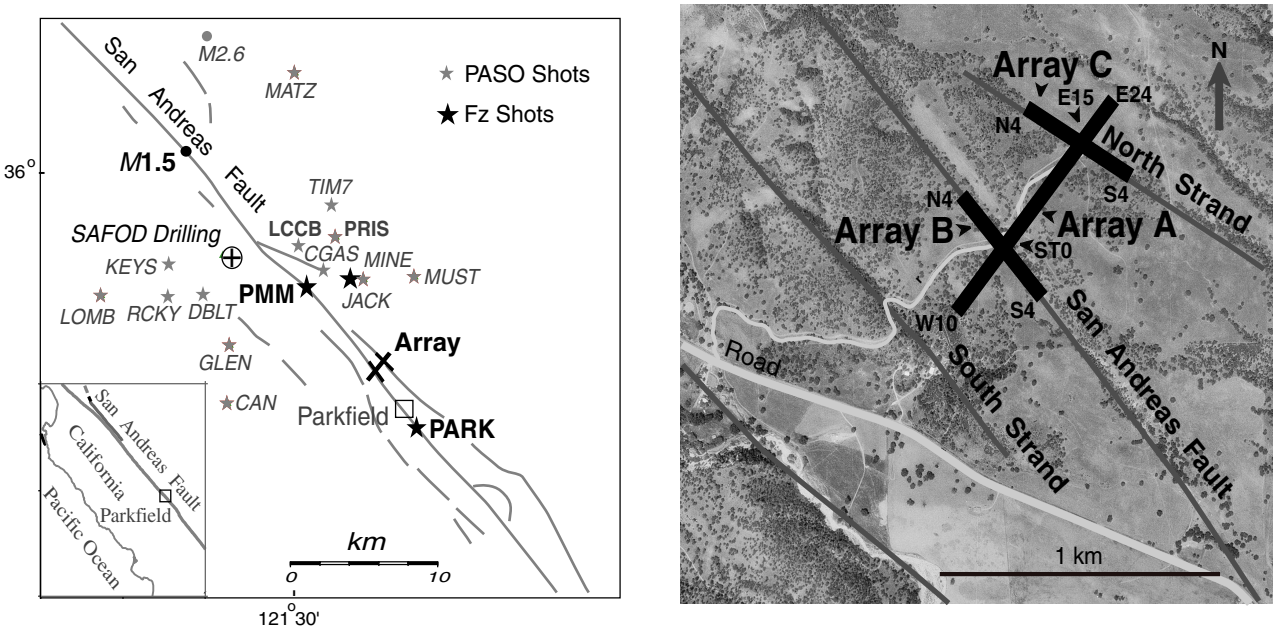

Figure 1 Top: Map shows locations of seismic arrays and shots at Parkfield, California in 2002. Black stars and bars – shots and arrays in fault-zone trapped wave study. Grey stars - shots in the PASO experiment. Dots – earthquakes recorded in this study. Bottom: Seismic arrays across and along the SAF. Array A consisted of 35 PASSCAL REFTEKs and three-component 2Hz sensors with station spacing of 25 m. Arrays B and C consisted of 9 REFTEKs for each with station spacing of 50 m. Stations located at fault traces and ends of arrays are labeled. Grey and white lines are fault surface traces and roads.

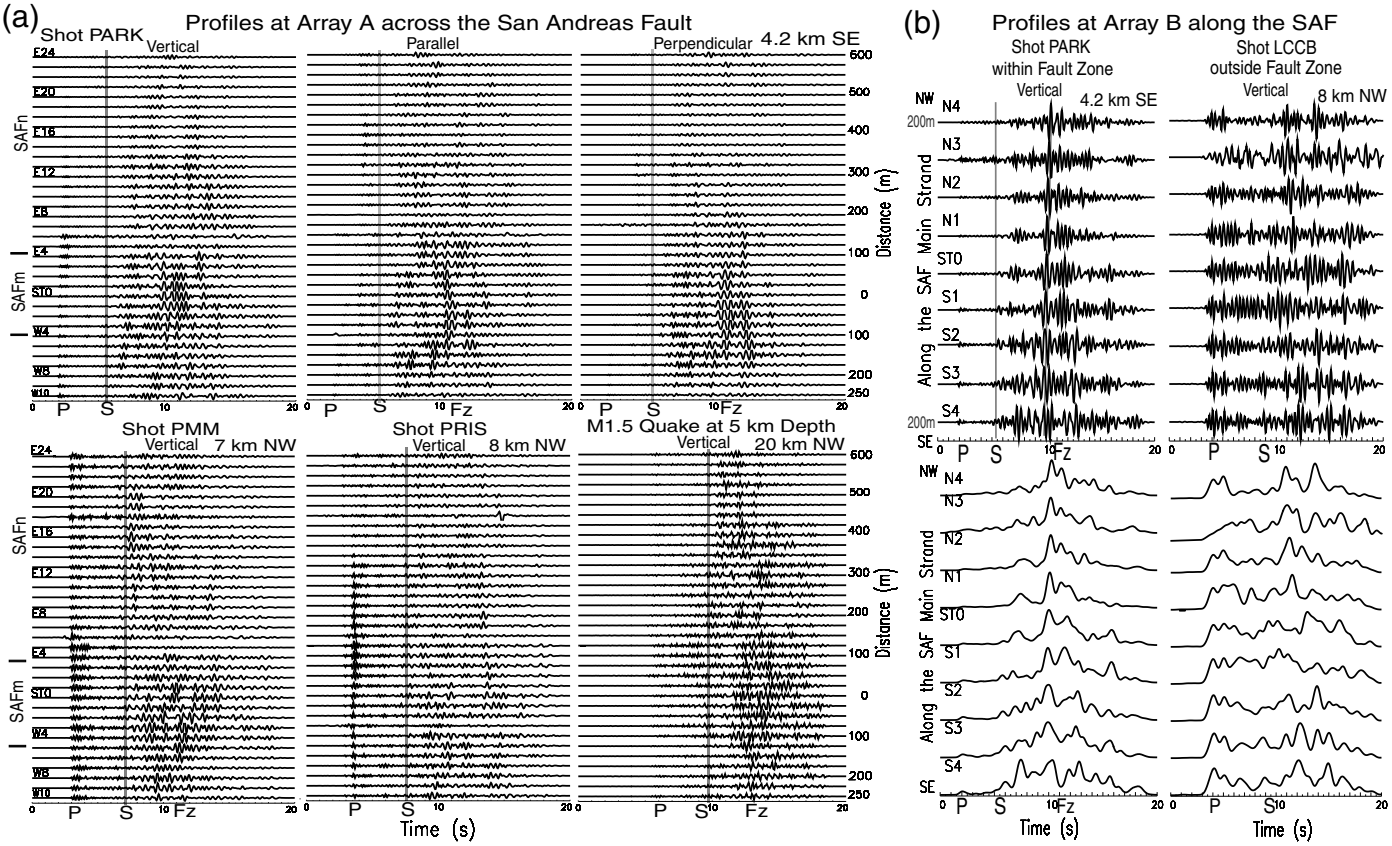

Figure 2 (a) Top: Three-component seismograms recorded at array A for shot PARK. Bottom: Vertical component seismograms at array A for shots PMM and PRIS, and a M1.5 quake at Parkfield. The distance between the array and events, station names and offsets are plotted. Stations ST0 and E15 were located on the main fault (SAFm) and north strand (SAFn). Seismograms have been filtered <4 Hz for shots and <5 Hz for the quake. Fault-zone trapped waves (Fz) are dominant at stations in the range marked by two bars for events on the SAF. (b) Vertical component seismograms and envelopes at array B for shots PARK and LCCB are trace -normalized in plots. Fz trapped waves with large amplitudes appeared after S arrivals for shot PARK.

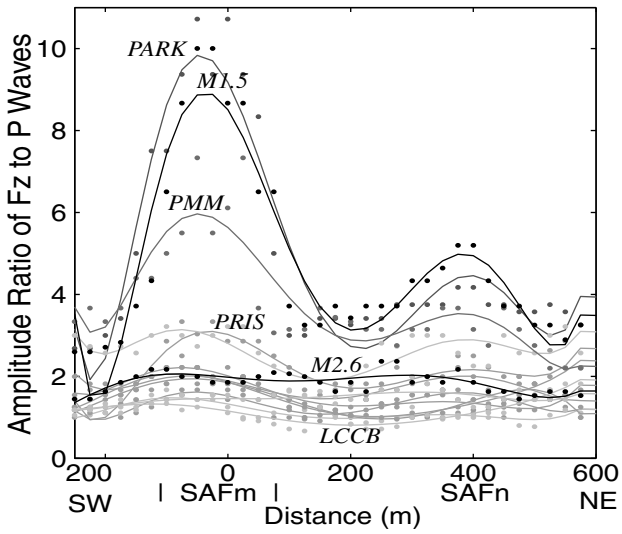

Figure 3 Computed amplitude ratios of fault-zone trapped waves to P waves at all stations of the 3 arrays for 12 shots and 2 earthquakes versus distance from the SAF main fault trace. Dots are the data points computed from amplitude ratios at all stations of 3 arrays for each event. Curves are a 5th-order polynomial fit to the data for each event. Selected events are labeled. The peak amplitude ratio is seen at stations close to the main fault for events located within the fault zone. In contract, amplitudes are flat at all stations for events away from the fault zone.

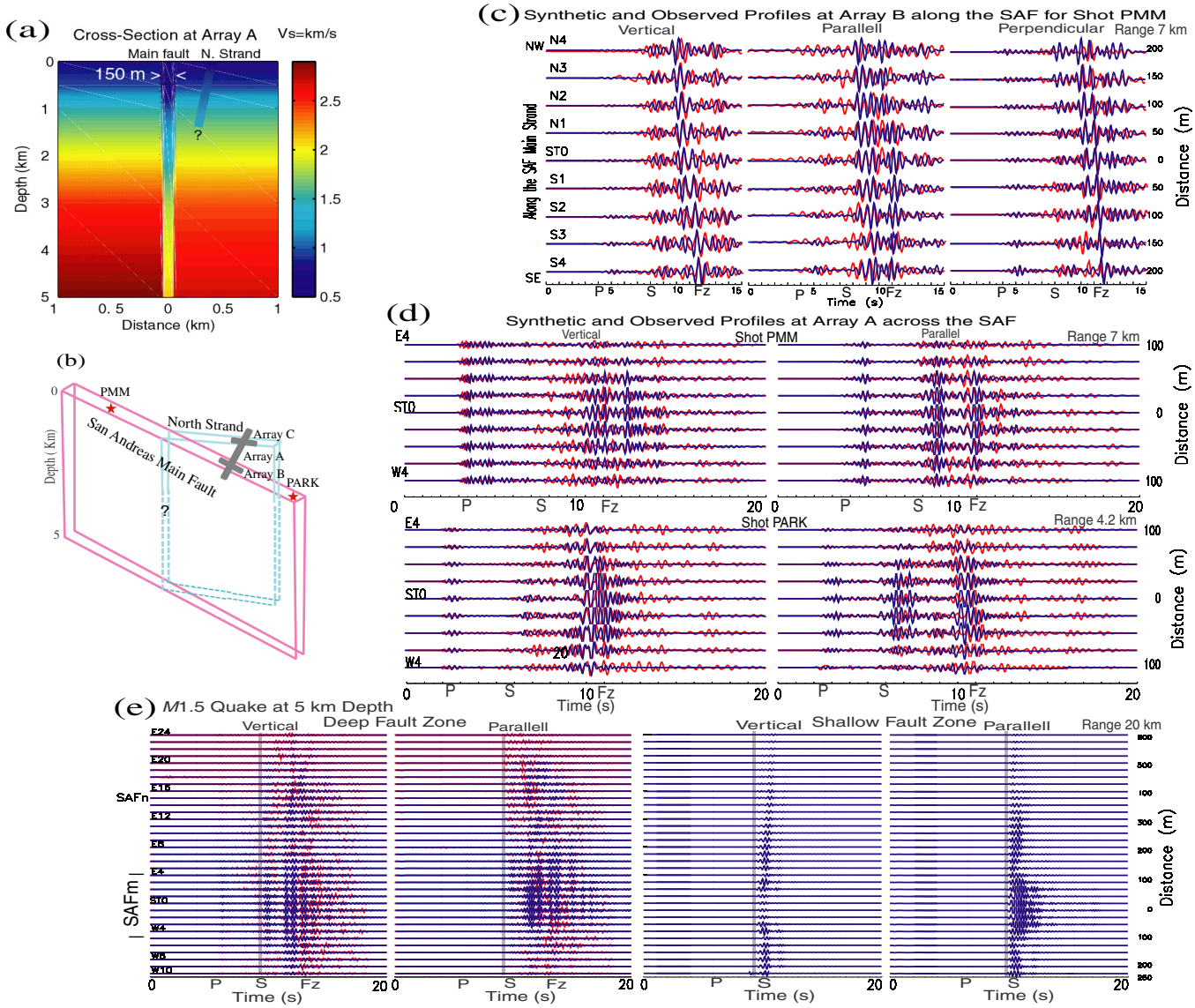

Figure 4 (a) Depth section of S velocities across the SAF at the array site. The main fault is marked by a ~150-m-wide low-velocity waveguide between the surface and 5 km depth. The north strand is marked by a minor waveguide. (b) The schematic fault planes at depths in the study area. (c) Observed (red lines) and synthetic (blue lines) seismograms at array B for shot PMM. Seismograms have been low-pass (<3 Hz) filtered and are trace-normalized in plots. An explosion source is located within the waveguide. (d) Same as in (c), but at stations of array A close to the main faultfor shots PMM and PARK. (e) Same as in (d), but at array A for the M1.5 quake. A double-couple source was located at the 5 km depth within the waveguide. Synthetic seismograms for a 1-km-deep shallow fault zone are show n for comparison withthose for the 5-km-deep fault zone.